



Integration of self-consistent polycrystal plasticity with dislocation density based hardening laws within an implicit finite element framework: Application to low-symmetry metals



Marko Knezevic^{a,b,*}, Rodney J. McCabe^a, Ricardo A. Lebensohn^a, Carlos N. Tomé^a, Cheng Liu^a, Manuel L. Lovato^a, Bogdan Mihaila^a

^a Materials Science and Technology Division, Los Alamos National Laboratory, Los Alamos, NM 87545, USA

^b Department of Mechanical Engineering, University of New Hampshire, Durham, NH 03824, USA

ARTICLE INFO

Article history:

Received 22 November 2012

Received in revised form

19 March 2013

Accepted 12 May 2013

Available online 6 June 2013

Keywords:

Uranium

Constitutive modeling

Finite element method

Texture

EBSD

ABSTRACT

We present an implementation of the viscoplastic self-consistent (VPSC) polycrystalline model in an implicit finite element (FE) framework, which accounts for a dislocation-based hardening law for multiple slip and twinning modes at the micro-scale grain level. The model is applied to simulate the macro-scale mechanical response of a highly anisotropic low-symmetry (orthorhombic) crystal structure. In this approach, a finite element integration point represents a polycrystalline material point and the meso-scale mechanical response is obtained by the mean-field VPSC homogenization scheme. We demonstrate the accuracy of the FE-VPSC model by analyzing the mechanical response and microstructure evolution of α -uranium samples under simple compression/tension and four-point bending tests. Predictions of the FE-VPSC simulations compare favorably with experimental measurements of geometrical changes and microstructure evolution. Specifically, the model captures accurately the tension–compression asymmetry of the material associated with twinning, as well as the rigidity of the material response along the hard-to-deform crystallographic orientations.

© 2013 Elsevier Ltd. All rights reserved.

1. Introduction

Polycrystal plasticity models such as Taylor-type (Kalidindi et al., 1992; Knezevic et al., 2009; Taylor, 1938; Van Houtte et al., 1999) and self-consistent-type models (Lebensohn and Tomé, 1993; Lebensohn et al., 2007) have been rigorously formulated and extensively used to understand and predict the mechanical response and microstructure evolution in metals subject to finite strains. The degree of sophistication necessary to accurately model a material generally depends on the crystal structure and the number and types of deformation modes active in the material. In this paper, we use α -uranium (α -U) as a model material system to illustrate the predictive capabilities of this modeling framework for low-symmetry metals. Uranium is an important metal for energy (e.g. metallic nuclear fuels) and defense applications, and is a challenging material to model because of its pronounced mechanical anisotropy. At room temperature, uranium has a low-symmetry

* Corresponding author at: Department of Mechanical Engineering, University of New Hampshire, 33 Academic Way, Kingsbury Hall, W119, Durham, NH 03824, USA. Tel.: +505 665 7587; fax: +505 667 8021.

E-mail address: marko.knezevic@unh.edu (M. Knezevic).

crystal structure (orthorhombic), and polycrystal plasticity requires activation of as many as four different slip modes, and at least two different deformation twinning modes. To complicate matters, the operating slip and twinning modes exhibit low multiplicity and widely different activation stresses. Consequently, the plastic response is highly anisotropic with marked tension–compression asymmetry and hardening depends strongly on texture and the interactions between the slip and twin modes. Recently, we showed that a hardening law explicitly based on dislocation density evolution implemented within the VPSC homogenization scheme performs well in capturing the anisotropic strain hardening and texture evolution in α -U (Knezevic et al., 2012; McCabe et al., 2010). Subsequently, the VPSC model of α -U was extended to account for strain-rate and temperature effects (Knezevic et al., 2013b). Comparison of simulations and experiments in these studies allowed us to infer basic information concerning the various slip and twin mechanisms, their interactions, and their role on strain hardening and texture evolution. It was found that the initial texture plays a significant role in determining the level of plastic anisotropy, and deformation twinning plays a major role in strain hardening behavior and texture evolution in α -U. Hence, it is evident that the accurate modeling of this complex material system requires a crystal-plasticity theoretical framework that accounts for microstructure evolution, rather than a continuum approach. These early successes provide the incentive for integrating the VPSC-based material subroutine for uranium into a finite element (FE) framework to facilitate predicting geometrical changes along with microstructure evolution of α -U components. Such integration is necessary for engineering structural and process modeling applications.

The strategy of embedding the mean-field VPSC model at the meso-scale level in an implicit FE analysis was recently discussed (Segurado et al., 2012). In an implicit nonlinear FE formulation, the material constitutive model provides the stress and tangent stiffness matrix. In our approach, the tangent stiffness matrix (Jacobian) is obtained analytically and allows for fast convergence towards stress equilibrium. The FE Jacobian is a function of the viscoplastic tangent moduli (which has already been calculated as part of the nonlinear self-consistent homogenization scheme), the elastic stiffness of the aggregate, and the FE time increment.

In this paper, we combine these recent advances and present an implementation of the VPSC polycrystalline model in implicit finite elements that accounts for a dislocation density based hardening law necessary to model the highly anisotropic response of α -U. We demonstrate that the VPSC calculations can be performed in the global FE frame rather than in the co-rotational frame adopted in the original FE-VPSC implementation (Segurado et al., 2012). The added benefit is that crystallographic texture stays in the global frame and thus the field and state variables are not regularly rotated between the global and co-rotational frame. Simple compression, simple tension, and simple shear tests on polycrystalline uranium are used to demonstrate the accuracy of the FE-VPSC model in ABAQUS by comparing with the results of the stand-alone VPSC model. The α -U FE-VPSC model is subsequently used to simulate the mechanical response and texture evolution of α -U cylinders in simple compression and beams in four-point bending deformation experiments. A total of two cylinders and four beams, classified by the alignment of the sample axis with respect to the rolled plate direction and the loading direction were experimentally deformed. Quantitative comparisons with experimental measurements of strain fields by digital image correlation (DIC) mapping, geometrical changes captured optically, and texture evolution by electron backscattered diffraction (EBSD) based orientation imaging are used to demonstrate the predictive capabilities of the model. We find that the FE-VPSC simulations capture well the strain field, shifts of the neutral axis of the beams, changes in the cross-section geometry and texture evolution during deformation.

2. Modeling framework

In this section, we outline the salient aspects of the micro-scale hardening law based on dislocation densities for α -U, the VPSC polycrystal plasticity meso-scale model and its implementation in the macro-scale implicit finite element framework.

2.1. Micro-scale model

Plastic deformation in each grain occurs via the activation of both slip and twin modes. The corresponding slip or twin shear rate, $\dot{\gamma}^s$ on a system, s , is given by the power-law:

$$\dot{\gamma}^s = \dot{\gamma}_0 \left| \frac{\boldsymbol{\sigma}' : \mathbf{m}^s}{\tau_c^s} \right|^{1/m} \text{sign}(\boldsymbol{\sigma}' : \mathbf{m}^s) \quad (1)$$

where $\boldsymbol{\sigma}'$ is the Cauchy stress deviator, \mathbf{m}^s is the Schmid tensor associated with slip or twinning system s , $\dot{\gamma}_0^s$ is the reference slip rate on system s , m is the rate sensitivity parameter, and τ_c^s is the resistance of slip or twinning system s . A rate-sensitivity exponent of 0.1 is taken to be the same for all slip and twinning modes.

Early experiments (Anderson and Bishop, 1962; Daniel et al., 1971; Fisher and McSkimin, 1958; Yoo, 1968) established the following four slip modes $(0\ 1\ 0)[1\ 0\ 0]$, $(0\ 0\ 1)[1\ 0\ 0]$, $\frac{1}{2}\{110\}\langle 1\bar{1}0\rangle$ and $\frac{1}{2}\{1\bar{1}2\}\langle 021\rangle$ to operate in α -U. In addition to slip, early studies (Cahn, 1951, 1953; Crocker, 1965; Daniel et al., 1971) confirmed the presence of several twin modes, the two most prevalent in wrought α -U being $\{130\}\langle 3\bar{1}0\rangle$ and $\{172\}\langle 3\bar{1}2\rangle$. Consistent with these experimental findings, we consider all of the above slip and twinning systems as potential systems for accommodating the imposed plastic strain in our model.

The equations underlying the single crystal dislocation density based hardening law implemented within VPSC were proposed in (Beyerlein and Tomé, 2008) and adopted for α -U in (Knezevic et al., 2012) and are briefly summarized here. τ_c^s of

all slip systems or twin variants within one mode α (or family) in a grain are assumed to exhibit the same resistance and they depend on the accumulated dislocation densities per slip mode. In the case of slip, τ_c^α is expressed as a sum of a friction stress, τ_o^α , a forest dislocation interaction stress, τ_{for}^α , and a dislocation substructure interaction stress, τ_{sub}^α , i.e.

$$\tau_c^\alpha = \tau_o^\alpha + \tau_{for}^\alpha + \tau_{sub}^\alpha \quad (2)$$

The evolution of τ_{for}^α and τ_{sub}^α is governed by the evolution of the forest ρ_{for}^α and substructure ρ_{sub}^α dislocation densities, as described below. The effect of forest dislocation density is given by a traditional Taylor law (Mecking and Kocks, 1981):

$$\tau_{for}^\alpha = \chi b^\alpha \mu^\alpha \sqrt{\rho_{for}^\alpha}, \quad (3)$$

where $\chi=0.9$ is a dislocation interaction parameter. Dislocation dynamics simulations show that the contribution to hardening by dislocations stored within substructure such as cell walls can be accounted for using (Maded et al., 2002)

$$\tau_{sub}^\alpha = k_{sub} \mu^\alpha b^\alpha \sqrt{\rho_{sub}^\alpha} \log\left(\frac{1}{b^\alpha \sqrt{\rho_{sub}^\alpha}}\right). \quad (4)$$

Here, $k_{sub}=0.086$ is an empirical parameter that recovers the Taylor law for low substructure dislocation densities (Maded et al., 2002).

The evolution of the stored forest density ρ_{for}^α is governed by competition between the rate of storage and the rate of dynamic recovery:

$$\frac{\partial \rho_{for}^\alpha}{\partial \gamma^\alpha} = \frac{\partial \rho_{gen,for}^\alpha}{\partial \gamma^\alpha} - \frac{\partial \rho_{rem,for}^\alpha}{\partial \gamma^\alpha} = k_1^\alpha \sqrt{\rho_{for}^\alpha} - k_2^\alpha(\dot{\epsilon}, T) \rho_{for}^\alpha, \quad \Delta \rho_{for}^\alpha = \frac{\partial \rho_{for}^\alpha}{\partial \gamma^\alpha} |\Delta \gamma^\alpha|, \quad (5)$$

where k_1^α is a rate-insensitive coefficient for dislocation storage by statistical trapping of gliding dislocations by forest obstacles and k_2^α is a rate-sensitive coefficient that accounts for dynamic recovery by thermally activated mechanisms. The latter coefficient, k_2^α , is given by (Beyerlein and Tomé, 2008)

$$\frac{k_2^\alpha}{k_1^\alpha} = \frac{\chi b^\alpha}{g^\alpha} \left(1 - \frac{kT}{D^\alpha b^3} \ln\left(\frac{\dot{\epsilon}}{\dot{\epsilon}_o}\right)\right). \quad (6)$$

In Eq. (6), k , $\dot{\epsilon}_o$, g^α , and D^α are the Boltzmann constant, a reference strain rate, an effective activation enthalpy and a drag stress, respectively. Dynamic recovery is often associated with thermal activation of dislocation cross-slip and climb, and the formation of dislocation sub-structures is concomitant with these recovery processes. As a consequence, in the model the rate of substructure development is coupled to the rate of recovery of all active dislocations through:

$$\Delta \rho_{sub} = \sum_\alpha q^\alpha b^\alpha \frac{\partial \rho_{rem,for}^\alpha}{\partial \gamma^\alpha} |\Delta \gamma^\alpha| \quad (7)$$

where q is a dislocation recovery rate coefficient defining the fraction of an α -type dislocations that do not annihilate but become substructure.

In the case of twinning, τ_c^β accounts for a temperature-independent friction term τ_o^β and a latent hardening term coupling slip and twin systems as:

$$\tau_c^\beta = \tau_o^\beta + \mu^\beta \sum_\beta C^{\alpha\beta} b^\beta b^\alpha \rho_{for}^\alpha. \quad (8)$$

Here μ^β , b^β and $C^{\alpha\beta}$ are the elastic shear modulus on the system, the Burgers vector or shear direction of a given system, and the latent hardening matrix, respectively. The twin transformation is modeled via the composite grain (CG) model (Proust et al., 2007). In brief, CG consists of identifying the twin system with the highest shear-rate among all active twin systems, i. e. the Predominant Twin System (PTS) in each grain, and partitioning the grain into a stack of flat ellipsoids having the crystallographic orientation of the predominant twin and the matrix, respectively. The short axis of the ellipsoids is perpendicular to the twin plane. As more shear is contributed by the twin, a volume fraction is transferred from the parent to the twin and the ellipsoids representing the twins thicken and the ones representing the parent shrink. Except for the volume transfer coupling, the twin and the parent ellipsoids are treated as independent inclusions in the model.

2.2. Meso-scale model

In order to obtain the mechanical behavior of polycrystalline α -U, we use a self-consistent model. This class of models is based on the solution of the problem of an ellipsoidal inclusion embedded in a homogenous effective medium. The inclusion is taken to be an individual grain while the homogenous medium represents the polycrystalline aggregate. A detailed description of the VPSC model used in this study can be found elsewhere (e.g. Lebensohn et al., 2007). Here we only report the equations necessary to follow the details of the FE implementation of the model.

The constitutive relations between the Cauchy stress deviator $\boldsymbol{\sigma}'$ and the viscoplastic strain-rate $\dot{\boldsymbol{\epsilon}}_{vp}$ at the single-crystal level at the special location \mathbf{x} are given by:

$$\dot{\boldsymbol{\epsilon}}_{vp}(\mathbf{x}) = \sum_{s=1}^{N_s} \mathbf{m}^s(\mathbf{x}) \dot{\gamma}^s(\mathbf{x}), \quad (9)$$

where the sum runs over all N_s slip and twin systems and \mathbf{m}^s is the Schmid tensor associated with the slip or twinning system s . A linear relation (an approximation of the actual local nonlinear relation, Eq. (9)) is assumed between $\dot{\boldsymbol{\epsilon}}_{vp}^{(r)}$ and $\boldsymbol{\sigma}'^{(r)}$, i.e.

$$\dot{\boldsymbol{\epsilon}}_{vp}^{(r)} = \mathbf{M}^{(r)} : \boldsymbol{\sigma}'^{(r)} + \dot{\boldsymbol{\epsilon}}^{o(r)} \quad (10)$$

where $\mathbf{M}^{(r)}$ and $\dot{\boldsymbol{\epsilon}}^{o(r)}$ are the linearized viscoplastic compliance and back-extrapolated strain-rate of grain r , respectively. The behavior of the single crystals can be homogenized assuming a linear relation at the effective medium (polycrystal, px) level:

$$\dot{\boldsymbol{\epsilon}}_{vp}^{(px)} = \mathbf{M}^{(px)} : \boldsymbol{\sigma}'^{(px)} + \dot{\boldsymbol{\epsilon}}^{o(px)} \quad (11)$$

where $\dot{\boldsymbol{\epsilon}}_{vp}^{(px)}$ and $\boldsymbol{\sigma}'^{(px)}$ are the effective (polycrystal) deviatoric strain-rate and stress tensors, respectively, and $\mathbf{M}^{(px)}$ and $\dot{\boldsymbol{\epsilon}}^{o(px)}$ are the tangent viscoplastic compliance and back-extrapolated strain-rate of an a priori unknown homogeneous linear medium that represents the behavior of the polycrystal. The usual procedure to obtain the homogenized response of a linear polycrystal is the linear self-consistent method. The problem underlying the self-consistent method is that of a single crystal r of moduli $\mathbf{M}^{(r)}$ and $\dot{\boldsymbol{\epsilon}}^{o(r)}$ embedded in an infinite medium of moduli $\mathbf{M}^{(px)}$ and $\dot{\boldsymbol{\epsilon}}^{o(px)}$, which can be obtained using standard self-consistent analysis. The linearization (Eqs. (10) and (11)) eventually lead to uniform stress and strain rate in the ellipsoidal domain of the grain.

The above numerical scheme is used to predict the stress–strain response and the microstructure evolution of the polycrystalline α -U (crystallographic and morphologic texture and hardening evolution), by applying the viscoplastic deformation to the polycrystal in incremental steps.

2.3. Macro-scale model

A finite element integration point is considered as a polycrystalline material point whose meso-scale mechanical response is obtained by interrogating the VPSC model described above. As a result, we introduce another level of homogenization from the meso-scale to the macro-scale. VPSC is implemented as a User Material Subroutine (UMAT) in ABAQUS Standard. The total strain increment $\Delta \boldsymbol{\epsilon}$ is divided into the elastic $\Delta \boldsymbol{\epsilon}_{el}$ and viscoplastic $\Delta \boldsymbol{\epsilon}_{vp}$ parts as:

$$\Delta \boldsymbol{\epsilon}^{(px)} = \Delta \boldsymbol{\epsilon}_{el}^{(px)} + \Delta \boldsymbol{\epsilon}_{vp}^{(px)} = \mathbf{C}^{-1} : \Delta \boldsymbol{\sigma}^{(px)} + \Delta \boldsymbol{\epsilon}_{vp}^{(px)} \quad (12)$$

where \mathbf{C} is the elastic stiffness of the polycrystalline material point, $\Delta \boldsymbol{\sigma}$ is the Cauchy stress increment, and $\Delta \boldsymbol{\epsilon}_{vp} = \Delta \boldsymbol{\epsilon}_{vp}(\boldsymbol{\sigma})$ is computed using the VPSC model for each polycrystalline material point. Note that superscript (px) is only used in Eq. (12) to show the continuity between the VPSC material point and the FE code and is explicitly dropped for simplicity. The elastic stiffness, \mathbf{C} , is computed using the elastic self-consistent (ELSC) estimate. Note that an ELSC calculation for the determination of \mathbf{C} is implemented in the VPSC code at the beginning of each deformation increment. Hence, the textural changes are also accounted for in determining the elastic modulus of the polycrystalline material element. The single-crystal elastic constants used for α -U are (Fisher, 1966; Fisher and McSkimin, 1958): $C_{11} = 214.8 \text{ GPa}$, $C_{22} = 198.6 \text{ GPa}$, $C_{33} = 267.1 \text{ GPa}$, $C_{44} = 124.4 \text{ GPa}$, $C_{55} = 73.4 \text{ GPa}$, $C_{66} = 74.3 \text{ GPa}$, $C_{12} = 46.5 \text{ GPa}$, $C_{13} = 21.8 \text{ GPa}$ and $C_{23} = 107.6 \text{ GPa}$.

In an earlier work (Segurado et al., 2012), the VPSC calculations were performed in a local co-rotational frame and the texture was represented in the same co-rotational frame. In our new implementation, the polycrystalline material undergoes macroscopic rotation due to the macroscopically imposed spin \mathbf{W}^{app} at every time increment. Therefore, each single crystal comprising the polycrystal undergoes rotation due to \mathbf{W}^{app} , in addition to a rotation due to the plastic spin \mathbf{W}^{pp} and antisymmetric part of the Eshelby tensor Π (Lebensohn et al., 2007). The macroscopically imposed spin \mathbf{W}^{app} can be computed from the increment of the macroscopic rotation $\Delta \mathbf{R}^{app}$ as $\mathbf{W}^{app} = \mathbf{N}\dot{\theta}$, where \mathbf{N} is the antisymmetric tensor expressed in terms of a dual vector \mathbf{n} whose components are obtained from $\Delta \mathbf{R}^{app}$ as follows: $n_1 = \Delta R_{32}^{app} - \Delta R_{23}^{app}$, $n_2 = \Delta R_{31}^{app} - \Delta R_{13}^{app}$, $n_3 = \Delta R_{21}^{app} - \Delta R_{12}^{app}$ and $\dot{\theta} = \arccos(1/2(\Delta R_{ii}^{app} - 1))/\Delta t$. The added benefit of the new implementation is that field and state variables stay in the global frame and are *not* regularly rotated between the global and co-rotational.

The macro-scale constitutive model is formulated incrementally:

$$\dot{\boldsymbol{\sigma}} = \mathbf{C} : (\dot{\boldsymbol{\epsilon}} - \dot{\boldsymbol{\epsilon}}_{vp}) \quad (13)$$

Integrating Eq. (13) from time t to $t + \Delta t$ gives:

$$\boldsymbol{\sigma} \Delta t = \mathbf{C} : (\Delta \boldsymbol{\epsilon} - \Delta \boldsymbol{\epsilon}_{vp}) \quad (14)$$

At the macroscopic level, the applied load is divided into increments, and the equilibrium at each increment is obtained by means of the FE analysis in an iterative fashion using a global nonlinear solver with the load increment controlled by time. Once the problem has been solved at time t , the solution for the next time increment requires the polycrystal model to provide a tangent stiffness (Jacobian) matrix $\mathbf{C}^{tg} = \partial \Delta \boldsymbol{\sigma} / \partial \Delta \boldsymbol{\epsilon}$ for each material point in order for the FE scheme to compute an initial guess for the nodal displacements at $t + \Delta t$. The strain increments obtained from that prediction at each material point, $\Delta \boldsymbol{\epsilon}^{FE}$,

together with the stress σ^t and the set of internal state variables corresponding to the previous increment are used inside UMAT to calculate a new guess for the stress and the Jacobian at $t+\Delta t$. When convergence in stress equilibrium is achieved by the global nonlinear scheme, the new values (at $t+\Delta t$) of the stresses, the internal variables, and the Jacobian matrix are accepted for every node, and the calculation advances to the next increment.

For a given $\Delta\epsilon^{FE}$, the VPSC-based UMAT is based on the minimization procedure described in (Segurado et al., 2012) and is summarized here. The elastic constitutive relation for the stress in the material point at $t+\Delta t$ is given by:

$$\sigma^{t+\Delta t} = \sigma^t + \mathbf{C} : \Delta\epsilon_{el} = \sigma^t + \mathbf{C} : (\Delta\epsilon - \Delta\epsilon_{vp}). \quad (15)$$

Using Eq. (15) and the viscoplastic constitutive relation, we obtain:

$$\Delta\epsilon = \mathbf{C}^{-1} : \Delta\sigma + \Delta t \dot{\epsilon}_{vp}^{(px)}(\sigma^t + \Delta\sigma) \quad (16)$$

For a given trial strain increment, $\Delta\epsilon^{FE}$, we define the residual $\mathbf{X}(\Delta\sigma)$ at each material point as a nonlinear function of the stress increment $\Delta\sigma = \sigma^{t+\Delta t} - \sigma^t$:

$$\mathbf{X}(\Delta\sigma) = \Delta\epsilon - \Delta\epsilon^{FE} = \mathbf{C}^{-1} : \Delta\sigma + \Delta t \dot{\epsilon}_{vp}^{(px)}(\sigma^t + \Delta\sigma) - \Delta\epsilon^{FE} \quad (17)$$

The condition $\mathbf{X}(\Delta\sigma) = 0$ (i.e. $\Delta\epsilon = \Delta\epsilon^{FE}$) is enforced using a Newton–Raphson (NR) scheme to solve the nonlinear system of equations. The corresponding Jacobian \mathbf{J}_{NR} is given by:

$$\frac{\partial \mathbf{X}(\Delta\sigma)}{\partial (\Delta\sigma)} = \mathbf{J}_{NR}(\Delta\sigma) = \mathbf{C}^{tg} = \mathbf{C}^{-1} + \Delta t \frac{\partial \dot{\epsilon}_{vp}^{(px)}}{\partial (\Delta\sigma)}(\sigma^t + \Delta\sigma; \beta_i^t) = \mathbf{C}^{-1} + \Delta t \mathbf{M}^{(px)}(\sigma^t + \Delta\sigma) \quad (18)$$

Hence, given a guess $\Delta\sigma^{k-1}$ for the stress increment, the new guess is obtained as:

$$\Delta\sigma^k = \Delta\sigma^{k-1} - \mathbf{J}_{NR}^{-1}(\Delta\sigma^{k-1}) : \mathbf{X}(\Delta\sigma^{k-1}) \quad (19)$$

In our formulation, the internal state variables such as crystallographic orientations, axis of the ellipsoids representing grain, orientation of these ellipsoids etc., β_i^t , are assumed explicit. The approach provides a closed expression for the FE Jacobian as a function of the viscoplastic tangent moduli (calculated as part of the VPSC algorithm), the elastic stiffness of the aggregate, and the FE time increment. The use of this expression greatly reduces the overall computational cost because the stress of the polycrystal and the elasto-viscoplastic tangent stiffness tensor are obtained from the same calculation loop. Moreover, the FE Jacobian allows for the quadratic convergence of the macroscopic nonlinear equations.

3. Applications of the FE-VPSC UMAT for low-symmetry metals

In the following we present several applications used to test the accuracy of the FE-VPSC model in ABAQUS. First, we compare directly the stress–strain response and texture predicted by the FE-VPSC model against the results obtained using the stand-alone SA-VPSC model. Next, we compare the predicted geometrical changes and texture evolution during simple compression and four-point beam bending with those measured experimentally. In all of the FE-VPSC simulations that follow, we use 3D finite elements. Finally, we discuss the effect of texture-induced anisotropy on material flow.

The material used here is straight-rolled polycrystalline α -uranium in its annealed condition. The processing route was described earlier (Knezevic et al., 2012). The microstructure and texture of the material before testing are shown in Fig. 1. The material has equiaxed twin-free grains with an average grain size of approximately 15 μm . The initial texture shown in Fig. 1 was measured by EBSD on a large area of several square millimeters to be representative of the material. The processing route of the starting material induced an orthotropic texture, which allows us to show only one quarter of the pole figures. The pole figures reveal that the material has a strong (001) texture component in the through-thickness (TT3) direction, tilted towards the in-plane 2 (IP2) direction. The (010) and (100) components tend to concentrate away from the (TT3) direction with the peak intensity for (010) being in the in-plane 1 (IP1) direction and the peak intensity for (100) being in the in-plane 2 (IP2) direction. The measured texture is reduced to 1000 orientations chosen such as to reproduce the experimental textures shown in Fig. 1. The pole figures of the texture used as input in the simulations are essentially indistinguishable from the experimental ones depicted in Fig. 1, and are not shown. Fig. 1 also shows the true-stress true-strain response of the α -U plate along the main rolling directions in simple compression and simple tension. Anisotropy and asymmetry of the mechanical response should be noted. The concave shape of the IPC1 and IPT2 curves is an indication of deformation twinning-dominated deformation. We observed in the earlier work (Knezevic et al., 2012) that twins in α -U grow rapidly inducing large texture hardening by re-orienting grain from a softer to a harder orientation while the Hall-Petch type hardening (due to grain subdivision) was minimal. For the comparison purpose, it is known that magnesium alloys exhibit a rapid growth of tensile twins resulting in large texture hardening (Knezevic et al., 2010). The TTC3, IPC2 and IPT1 curves show a classical decreasing hardening rate throughout, which is a sign that the plastic deformation is dominated by slip. The VPSC constitutive parameters for the material were calibrated in the previous study on the same material (Knezevic et al., 2012 see Tables 2 and 3) and are used in this study.

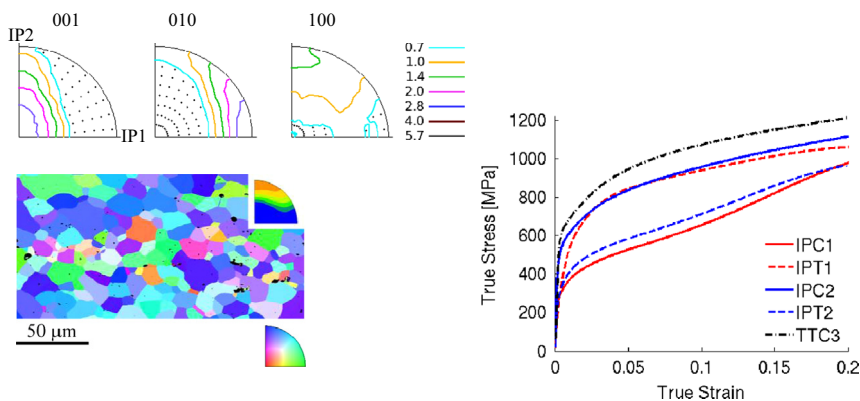


Fig. 1. Pole figures and EBSD orientation map showing initial microstructure and texture in the as-annealed straight-rolled uranium. The colors in the map indicate the crystal direction parallel to the IP1 direction (unit triangle at the bottom). In the corner of the map we illustrate the inverse pole figure for the IP1 direction. The IPF triangle has the crystal reference frame defined as [1 0 0] bottom right, [0 1 0] top left, and [0 0 1] bottom left. Stress-strain response in compression (C) and tension (T) at room temperature is shown along the directions indicated in the plot of annealed α -uranium. (For interpretation of the references to color in this figure caption, the reader is referred to the web version of this article.)

3.1. Validation of FE-VPSC with SA-VPSC

For the purpose of validation, we compare the results of the FE-VPSC UMAT implementation against those of the SA-VPSC model with simple boundary conditions, i.e. the type of imposed boundary conditions the SA-VPSC model can handle. Simple tension and simple compression up to a strain of 0.2 are simulated using SA-VPSC by imposing 0.002 strain increments along the corresponding direction, while enforcing zero average stress along the two lateral directions of the sample. The same tests were simulated with the FE-VPSC UMAT and compared with the SA-VPSC model results. We constructed the simple FE models of single linear element C3D8 (8 nodes, and 8 integration points) with displacements imposed along the 2-direction for compression and tension and stress-free boundary conditions on the lateral faces. In addition, simple shear tests were performed by SA-VPSC as well as FE-VPSC where the same one element model was used. We applied deformation gradient of $\mathbf{F} = \mathbf{I} + \gamma \mathbf{e}_2 \otimes \mathbf{e}_3$, with $\gamma = 0.2$. This analysis was performed in order to check the correct treatment of rotations under finite-deformation kinematics. The predicted stress-strain curves and pole figures predicted by the two models are in excellent agreement (see Fig. 2). Observe that SA-VPSC does not produce the elastic response, which causes some difference with FE-VPSC.

3.2. Compression of α -uranium

Simple compression experiments were performed on cylinders machined from the straight-rolled α -U plate in two different directions, the rolling direction (IPC1) and the through-thickness direction (TTC3). These tests were also used to validate the implemented FE-VPSC UMAT and illustrate the effect of texture-induced anisotropy on the mechanical response of α -U. The FE model consisted of approximately 1000C3D8 elements with the same 1000 grains at each integration point (see Fig. 1). The geometrical changes of the samples compressed to a strain of 0.2 are shown in Fig. 3. Here, the symbols overlaid onto the photographs of the deformed cross sections denote the external nodal coordinates of the deformed FE model predictions. Note that the TTC3 compressed cylinder preserves a near uniform cross-section and the IPC1 compressed cylinder developed an oval cross-section. The accuracy of our simulation results relative to the geometrical changes measured experimentally, demonstrate that the FE-VPSC UMAT implementation accurately predicts the complex deformation behavior (i.e. texture-induced anisotropic material flow) exhibited by α -U. The measured and simulated horizontal and vertical strains are in excellent agreement and are about 0.092 and 0.084 for the cylinder compressed in the direction 3 and 0.074 and 0.110 for the cylinder compressed in the direction 1. Computational time associated with a uniaxial deformation simulation involving 1000 elements containing 1000 grains up to a strain of 0.2 is about 60 h on a regular PC. However our implementation can run in parallel and a multiple CPU hardware can substantially reduce the time involved.

3.3. Bending of α -uranium

A detailed evaluation of the FE-VPSC model is presented by comparing the model predictions with the experimental measurements of dimensional changes and microstructure evolution during the four-point bending of α -U beams. Four-point beam bending tests present more stringent tests of the model, as one produces a continuous gradient of strain, from compressive conditions in the upper portion to tensile conditions in the bottom portion of the beams. These conditions were selected for validation of the FE-VPSC models capabilities to predict the effects of the directionality of twinning.

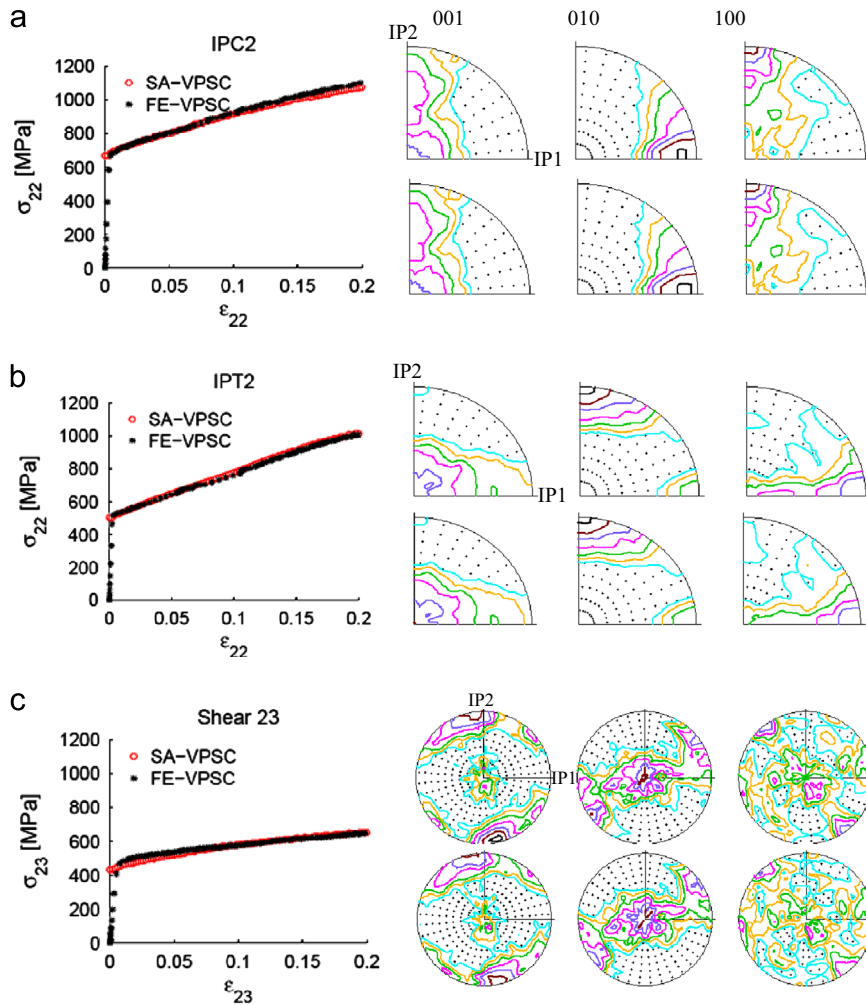


Fig. 2. Predictions of the FE-VPSC UMAT described here compared with the corresponding predictions of SA-VPSC for (a) in-plane compression in 2 direction (IPC2), (b) in-plane tension in 2 direction (IPT2) and (c) simple shear in 23 direction of α -uranium: stress-strain curves and pole figures at strain of 0.2 (SA-VPSC top row and FE-VPSC bottom row). The intensity of the contour lines corresponds to 0.7/1.0/1.4/2.0/2.8/4.0/5.7 (see Fig. 1 for colors).

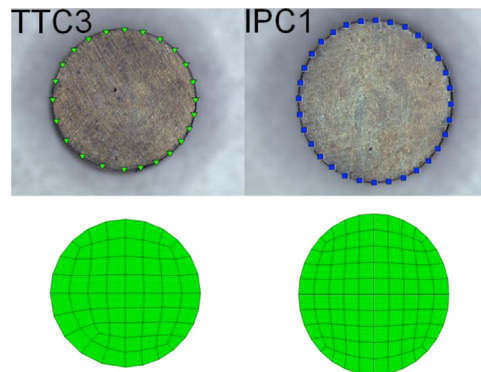


Fig. 3. Comparison of the predictions using the FE-VPSC UMAT and experimentally measured cross-sections of cylinders compressed up to a strain of 0.2 in the direction 3 (on the left) and in the direction 1 (on the right). The external nodal coordinates of the deformed FEM model are superimposed on the experimentally deformed samples of uranium.

Depending on the loading direction with respect with to the texture in the beams, we expect to find qualitative differences between the response of the upper (top/compressive) and lower (bottom/tensile) portions of the beam and a shift of the neutral axis. We also provide insights into deformation behavior of α -U during bending.

The photograph of the four-point beam testing jig with the test specimen is shown in Fig. 4. We followed the same experimental setup as in our earlier work involving titanium (Knezevic et al., 2013a; Nixon et al., 2010). It consisted of a pair of internal pins, moving downwards from the top of the beam, and a pair of external pins, fixed underneath the beam. The internal and external pairs of pins were set at center-to-center distances of ± 6.35 mm and ± 19.05 mm, respectively. The total displacement of the upper pins was -3.5 mm, corresponding to an axial (longitudinal) strain of the most external fiber of approximately 0.1. The deformed specimens were cut at the midpoint and the final deformed cross-sections photographed. The photographed cross-sections are used to test the accuracy of the FE-VPSC model. Four specimens machined from the orthotropic plate of α -U were tested along different loading orientations. Specifically, two samples had the beam axis aligned with the plate IP1, while the other two samples had the beam axis aligned with the plate IP2. For each of these two sets of specimens, one sample was loaded in the TT3 direction while the other sample was loaded in the other in-plane direction normal to the beam axis. As a result, the beams had different starting textures relative to the bending plane. Our aim is to illustrate the ability of the FE-VPSC model to capture the strong effect of texture-induced anisotropy and asymmetry on the geometrical changes during bending of α -U. The four test configurations are shown in Fig. 5. We show the experimentally deformed beams, together with the model results. The predicted axial strain distributions are shown. Each beam had a square cross-section of 6.35 mm \times 6.35 mm and a length of 50.8 mm.

Due to the presence of orthotropic symmetry, we only model a quarter of the beam using a structured mesh of $20 \times 5 \times 3$ elements along the half-length, thickness and half-width, respectively by imposing symmetry boundary conditions. The displacement of the upper pins was modeled by imposing displacement corresponding to experimental values along the loading direction to the upper nodes, located at 6.35 mm from the midpoint. The lower nodes, located at 19.05 mm from the midpoint are constrained along the loading direction (no displacement is allowed along the loading direction) to represent the fixed pins.

After performing a mesh-sensitivity study, we observed that further refinement of the mesh leaves the results unchanged and adding more elements only increased the computational time involved. We found that the quadratic elements with reduced integration (C3D20R) provided the best compromise between accuracy of the simulations and the computational time involved. These elements were flexible to bend owing to the large number of degrees of freedom (20 nodes) and efficient owing to the reduced number of integration points where the computationally intensive polycrystalline response is obtained.

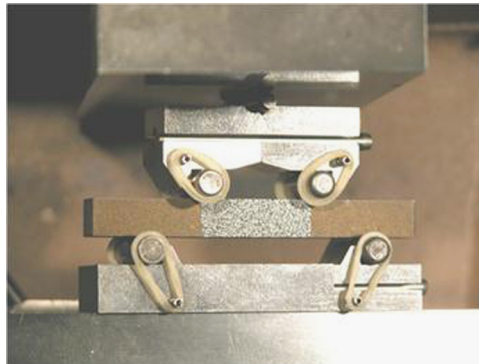


Fig. 4. Four-point beam testing jig with a test specimen.

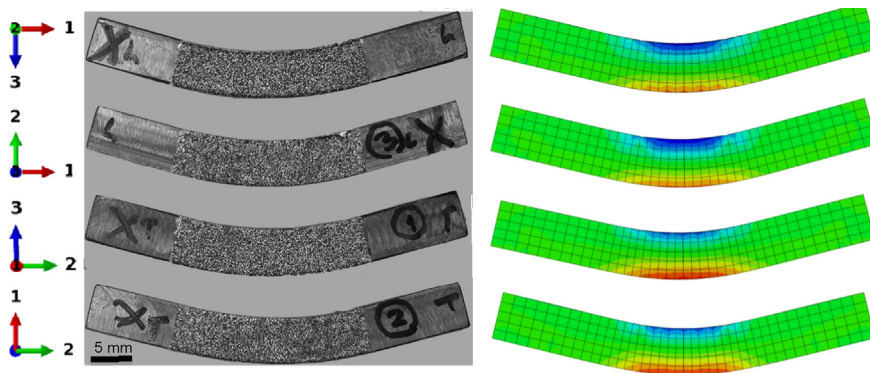


Fig. 5. Test configurations of the four-point beam bending specimens with a sprayed speckle pattern for DIC measurements (left) and corresponding FE models showing the axial strain distributions (right). The long axis of the specimens and the loading direction align with the directions of the α -U plate, as follows: 1=IP1, 2=IP2 and 3=TT3.

In Fig. 6 we illustrate the comparison between the predicted and measured cross sections of the α -U beams in the final deformed state. Here, the symbols overlaid onto the photographs of the deformed cross sections denote the external nodal coordinates of the deformed FE model predictions and show that the FE-VPSC model accurately predicts the dimensional changes of the cross sections for all cases considered here. The model predicts the deviation of the final cross section from the initial square shape of the cross section of the beam. This deviation depends on the corresponding beam configuration and deformation direction and reflects the anisotropic character of the mechanical response in α -U induced by the strong effect of texture. Note that when the through-thickness direction (TT) is perpendicular to the loading direction, the cross-sections of the beams retain an almost square shape, because it is difficult to deform the material along the $\langle 001 \rangle$ direction. In turn, the samples deformed in-plane developed wedge-shape cross sections, with more lateral strain when the IP1 of the plate is horizontal. This is consistent with the uniaxial tests results shown in Fig. 1, which show that the IP1 direction is softer than the IP2 direction of the α -U plate. The results also emphasize the importance of the anisotropy of the macroscopic plastic Poisson strain. When a compressive or tensile deformation in a grain result in twinning, the resulting Poisson strain is in a direction perpendicular to $\langle 001 \rangle$ because of the crystallography of the twins. When the beams are loaded parallel with TT3, the resulting Poisson strain anisotropy largely occurs in the horizontal cross-section direction resulting in the changes in shape. Below, we explain this in more detail.

As indicated in Fig. 5, speckle patterns were sprayed on one side of each beam and local strain measurements were obtained using the digital image correlation (DIC) technique (Rastogi et al., 2000). The experimentally measured and predicted strain fields in the final deformed beams are illustrated in Fig. 7, together with the corresponding experimental

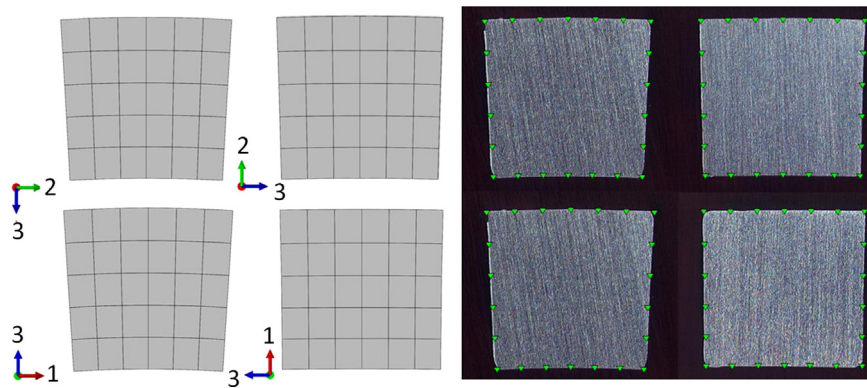


Fig. 6. Comparison of the predicted and measured cross-sections of the α -uranium beams. The external nodal coordinates of the deformed FEM models are superimposed on the photographed experimentally deformed beams.

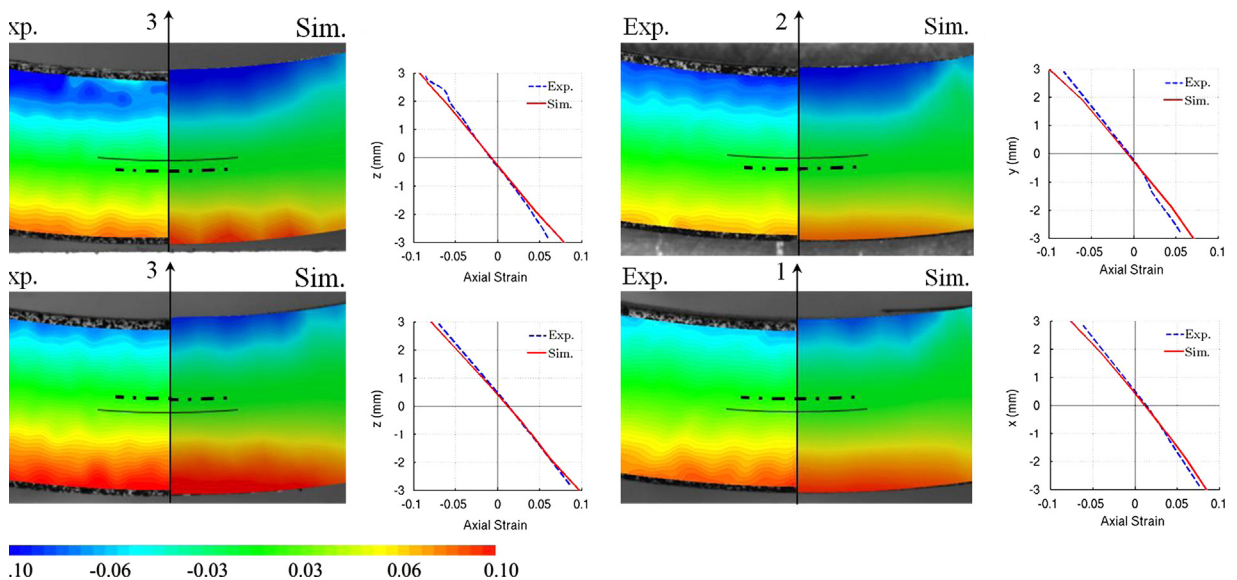


Fig. 7. Comparison of the axial strain contours and the axial strains along the height of the beams simulated with the FE-VPSC against DIC data. Note the shift in the neutral axis of the beams. The lines are the geometric center lines and the dotted curves are the neutral axis lines.

and calculated height dependence of the axial strains at the center of the beams. There is a downward shift of the neutral axis when the beam axis is aligned with the RD direction of the plate, which is a consequence of the material being harder in tension than in compression. Likewise there is an upward shift of the neutral axis when the beam axis is aligned with the TD

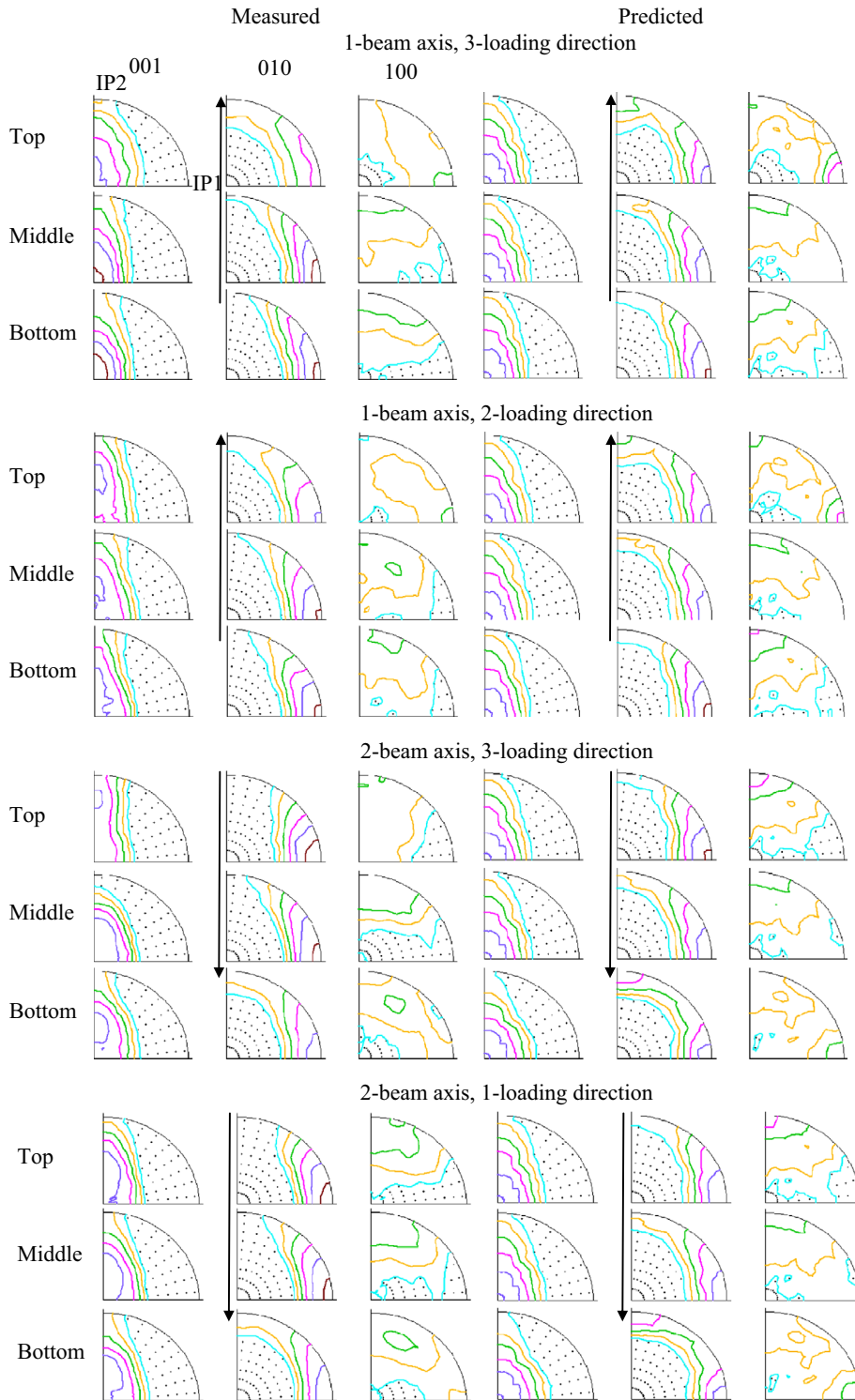


Fig. 8. Pole figures showing measured (on the left) and predicted (on the right) texture at the top, middle, and bottom locations for each α -uranium beam at the end of the bending deformation. Arrow indicates the change in the (010) texture component due to twinning as a function of beam height. The intensity of the contour lines corresponds to 0.7/1.0/1.4/2.0/2.8/4.0/5.7 (see Fig. 1 for colors).

direction of the plate, due to the material being softer in tension than in compression. Again, the agreement of the FE-VPSC model predictions and the experimental observations is excellent in all four cases considered here.

Fig. 8 shows the measured and predicted texture evolution of the material. We find that when the beam axis is aligned with the plate IP1 direction, the (010) peak intensity becomes stronger in the IP2 direction (and weaker in the IP1 direction)

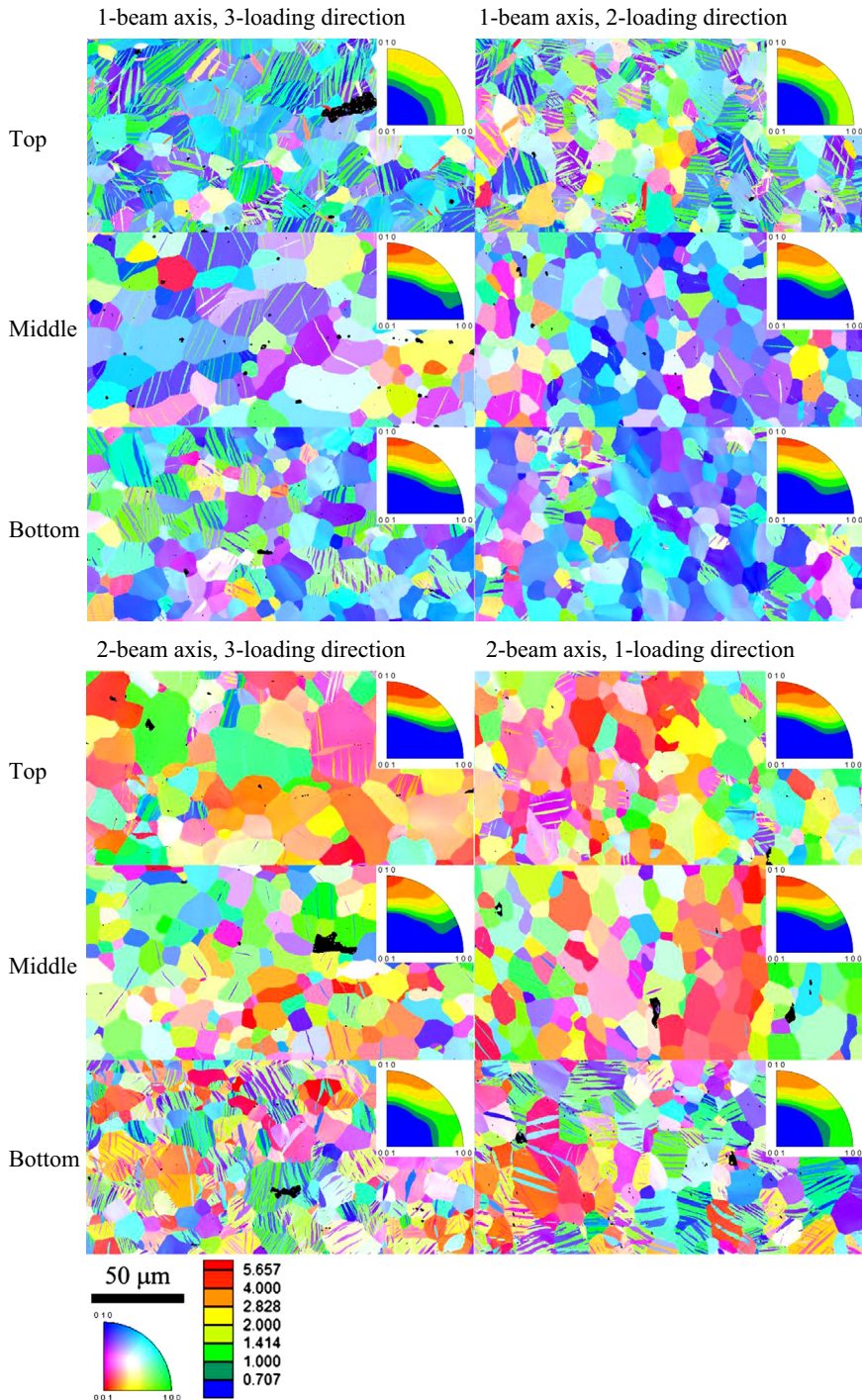


Fig. 9. Inverse pole figure (IPF) maps showing microstructure evolution in the α -uranium beams at the top, middle, and bottom locations for each beam at the end of the bending deformation. The middle images were taken at the geometric centers of the beams and the top and bottom were ± 3 mm from the geometric centers. The colors in these maps indicate the direction of the beam axis with respect to the crystal reference frame. The IPF texture plots in the upper right corner of each image indicate intensities in the IP1 direction. (For interpretation of the references to color in this figure caption, the reader is referred to the web version of this article.)

due to twinning in the top compressive portion of the beam (see the IPC1 stress–strain response in Fig. 1). Likewise, when the beam axis is aligned with the IP2, the (010) peak intensity becomes stronger in the IP1 direction (and weaker in the IP2 direction) due to twinning in the bottom portion of the beam experiencing a tensile stress state (see the IPT2 stress–strain response in Fig. 1). These trends in texture change due to twinning are indicated in the Fig. 8 by a line with an arrow. In the middle of the beam there is very little texture change, and the texture is expected to be the same as the initial texture. However, due to a small size of EBSD scans taken to measure texture along the height of the beams compared to a very large EBSD scan taken to measure the initial texture in the Fig. 1, the textures in the middle of the beams are not exactly the same as the one shown in the Fig. 1, but they are very similar. We associate the small difference between the measured and the predicted textures shown in the Fig. 8 to the smaller size of the EBSD scans that are perhaps not statistically representative of the texture in the beams. We reiterate that in the simulations we used the initial texture shown in the Fig. 1, obtained from a very large EBSD scan. Qualitatively, the measured and the predicted changes in the textures in the top portion of the beams and in the bottom portion of the beams relative to the texture in the middle of the beams (if we assume that the textures in the middle of the beams were not changing) are in excellent agreement. The twinning activity is further illustrated in the Fig. 9. The inverse pole figures also show the trend in the texture evolution in the beams as a function of height. We observe that the orientation of the twin lamellas varies with the configurations of the beams. When most of the twins are oriented vertically, the horizontal flaw of the material is possible through thickening/growth of the twins. Most of the twins observed in Fig. 9 are $\{130\}\langle 3\bar{1}0\rangle$ twins. The twin plane $\{130\}$ and shear direction $\langle 3\bar{1}0\rangle$ are perpendicular to the $[0\ 0\ 1]$ direction. For compression, the shear produced by a $\{130\}\langle 3\bar{1}0\rangle$ twin results in contraction along the compression direction (usually close to a $(0\ 1\ 0)$) and a macroscopic plastic Poisson extension in the direction perpendicular to both the compression direction and the $[0\ 0\ 1]$ direction (usually close to a $(1\ 0\ 0)$). Similarly for compression, the shear produced by a $\{130\}\langle 3\bar{1}0\rangle$ twin results extension along the tension direction (usually close to a $(1\ 0\ 0)$) and a Poisson contraction in the direction perpendicular to both the tension direction and the $[0\ 0\ 1]$ direction (usually close to a $(0\ 1\ 0)$). Because of the strong starting textures, this effect results in an anisotropic Poisson strain effect culminating in the different shapes observed in Fig. 6, which the model captures well.

Future work will concentrate on extending the hardening law to include effects such as reverse dislocation motion (Kitayama et al., *in press*) and de-twinning (Proust et al., 2008), which are important to account for by the model to be able to perform full-scale performance evaluations of uranium components where any kind of non-proportional loading can be expected and on applications of the modeling framework developed here in microstructure design (Fast et al., 2008; Kalidindi et al., 2009; Knezevic and Kalidindi, *in press*) and process design (Knezevic et al., 2008; Shaffer et al., 2010) for uranium components.

4. Conclusions

In this paper we discuss the numerical implementation of a recent VPSC polycrystalline model for low-symmetry metals into an FE framework. The VPSC model uses a dislocation density based hardening law and is able to predict the highly anisotropic mechanical response of low-symmetry metals. We showed that the FE-VPSC implementation can be simplified by performing calculations in the global frame rather than in the co-rotational frame adopted in the original FE-VPSC implementation. First, we verified that the FE-VPSC model reproduces the results of the stand-alone SA-VPSC model for simple compression, simple tension, and simple shear tests on polycrystalline wrought α -uranium (orthorhombic crystal structure). Then, the FE-VPSC model was used to simulate the dimensional changes and microstructure evolution in simple compression and four-point bending tests. We showed that the model successfully predicts the deformed shape of the cylinders and the beam cross sections by direct comparison with experiments performed on α -uranium samples. In addition, we demonstrated that the strain fields measured experimentally by digital image correlation strain mapping compare well with the strain fields predicted by the FE-VPSC model in the final deformed beams. Similarly, we find good agreement between the corresponding experimental and calculated height dependence of the axial strains at the center of the beams. Finally, we show a good agreement of the predicted and measured texture evolution as a function of beam height. Keeping in mind that the VPSC constitutive law was adjusted previously to an independent set of monotonic experiments, we emphasize that no additional knobs were available in order to affect the material response in the FE-VPSC simulations, and the results of the simulations should be regarded as predictions in that sense. Therefore, we conclude that the FE-VPSC model is able to capture with great accuracy the evolution of anisotropy and tension–compression asymmetry of the material due to microstructure evolution, as well as the rigidity of the material flow along hard-to-deform crystallographic directions.

Acknowledgements

This work was supported in part by the US Department of Energy under contract number DE-AC52-06NA25396. M. Knezevic gratefully acknowledges the Seaborg Institute for partial financial support under a Post-Doctoral Fellowship through the LANL LDRD Program. The EBSD work was performed in the electron microscopy laboratory (EML) at Los Alamos. The authors acknowledge T. Beard for help with mechanical testing and J. Crapps for help with setting up the FE model.

References

- Anderson, R.G., Bishop, J.W. 1962. The effect of neutron irradiation and thermal cycling on permanent deformations in uranium under load. In: Symposium on uranium and graphite. The Institute of Metals, London, 17–23.
- Beyerlein, I.J., Tomé, C.N., 2008. A dislocation-based constitutive law for pure Zr including temperature effects. *Int. J. Plasticity* 24, 867–895.
- Cahn, R.W., 1951. Twinning and slip in α -uranium. *Acta Crystallogr.* 4, 470.
- Cahn, R.W., 1953. Plastic deformation of alpha-uranium; twinning and slip. *Acta Metall.* 1 (49–52), 53–70. IN41-IN45.
- Crocker, A.G., 1965. The crystallography of deformation twinning in alpha-uranium. *J. Nucl. Mater.* 16, 306–326.
- Daniel, J.S., Lesage, B., Lacombe, P., 1971. The influence of temperature on slip and twinning in uranium. *Acta Metall.* 19, 163–173.
- Fast, T., Knezevic, M., Kalidindi, S.R., 2008. Application of microstructure sensitive design to structural components produced from hexagonal polycrystalline metals. *Comput. Mater. Sci.* 43, 374–383.
- Fisher, E.S., 1966. Temperature dependence of the elastic moduli in alpha uranium single crystals, part IV (298 to 923 K). *J. Nucl. Mater.* 18, 39–54.
- Fisher, E.S., McSkimin, H.J., 1958. Adiabatic elastic moduli of single crystal alpha Uranium. *J. Appl. Phys.* 29, 1473–1484.
- Kalidindi, S.R., Bronkhorst, C.A., Anand, L., 1992. Crystallographic texture evolution in bulk deformation processing of Fcc metals. *J. Mech. Phys. Solids* 40, 537–569.
- Kalidindi, S.R., Knezevic, M., Niezgodza, S., Shaffer, J., 2009. Representation of the orientation distribution function and computation of first-order elastic properties closures using discrete Fourier transforms. *Acta Mater.* 57, 3916–3923.
- Kitayama, K., Tomé, C.N., Rauch, E.F., Gracio, J.J., Barlat, F., A crystallographic dislocation model for describing hardening of polycrystals during strain path changes. Application to low carbon steels. *Int. J. Plast.* 54–69, <http://dx.doi.org/10.1016/j.ijplas.2012.09.004>, in press.
- Knezevic, M., Al-Harbi, H.F., Kalidindi, S.R., 2009. Crystal plasticity simulations using discrete Fourier transforms. *Acta Mater.* 57, 1777–1784.
- Knezevic, M., Capolungo, L., Tomé, C.N., Lebensohn, R.A., Alexander, D.J., Mihaila, B., McCabe, R.J., 2012. Anisotropic stress-strain response and microstructure evolution of textured α -uranium. *Acta Mater.* 60, 702–715.
- Knezevic, M., Kalidindi, S.R., Fast computation of first-order elastic-plastic closures for polycrystalline cubic-orthorhombic microstructures. *Comput. Mater. Sci.* 643–648, <http://dx.doi.org/10.1016/j.commatsci.2006.08.025>, in press.
- Knezevic, M., Kalidindi, S.R., Mishra, R.K., 2008. Delineation of first-order closures for plastic properties requiring explicit consideration of strain hardening and crystallographic texture evolution. *Int. J. Plasticity* 24, 327–342.
- Knezevic, M., Lebensohn, R.A., Cazzacu, O., Revil-Baudard, B., Proust, G.n.l., Vogel, S.C., Nixon, M.E., 2013a. Modeling bending of α -titanium with embedded polycrystal plasticity in implicit finite elements. *Mater. Sci. Eng. A* 564, 116–126.
- Knezevic, M., Levinson, A., Harris, R., Mishra, R.K., Doherty, R.D., Kalidindi, S.R., 2010. Deformation twinning in AZ31: influence on strain hardening and texture evolution. *Acta Mater.* 58, 6230–6242.
- Knezevic, M., McCabe, R.J., Tomé, C.N., Lebensohn, R.A., Chen, S.R., Cady, C.M., Gray III, G.T., Mihaila, B., 2013b. Modeling mechanical response and texture evolution of α -uranium as a function of strain rate and temperature using polycrystal plasticity. *Int. J. Plasticity* 43, 70–84.
- Lebensohn, R.A., Tomé, C.N., 1993. A self-consistent anisotropic approach for the simulation of plastic deformation and texture development of polycrystals: Application to zirconium alloys. *Acta Metall. Mater.* 41, 2611–2624.
- Lebensohn, R.A., Tomé, C.N., Castaneda, P.P., 2007. Self-consistent modelling of the mechanical behaviour of viscoplastic polycrystals incorporating intragranular field fluctuations. *Philos. Mag.* 87, 4287–4322.
- Madec, R., Devincere, B., Kubin, L.P., 2002. From dislocation junctions to forest hardening. *Phys. Rev. Lett.* 89, 255508.
- McCabe, R.J., Capolungo, L., Marshall, P.E., Cady, C.M., Tomé, C.N., 2010. Deformation of wrought uranium: experiments and modeling. *Acta Mater.* 58, 5447–5459.
- Mecking, H., Kocks, U.F., 1981. Kinetics of flow and strain-hardening. *Acta Metall. Mater.* 29, 1865–1875.
- Nixon, M.E., Lebensohn, R.A., Cazzacu, O., Liu, C., 2010. Experimental and finite-element analysis of the anisotropic response of high-purity α -titanium in bending. *Acta Mater.* 58, 5759–5767.
- Proust, G., Tomé, C.N., Jain, A., Agnew, S.R., 2008. Modeling the effect of twinning and detwinning during strain-path changes in magnesium alloy AZ31. *Int. J. Plasticity* 25, 861–880.
- Proust, G., Tomé, C.N., Kaschner, G.C., 2007. Modeling texture, twinning and hardening evolution during deformation of hexagonal materials. *Acta Mater.* 55, 2137–2148.
- Rastogi, P., Sutton, M., McNeill, S., Helm, J., Chao, Y. 2000. Advances in two-dimensional and three-dimensional computer vision, In: *Photomechanics*. Springer, Berlin Heidelberg, 323–372.
- Segurado, J., Lebensohn, R.A., Llorca, J., Tomé, C.N., 2012. Multiscale modeling of plasticity based on embedding the viscoplastic self-consistent formulation in implicit finite elements. *Int. J. Plasticity* 28, 124–140.
- Shaffer, J.B., Knezevic, M., Kalidindi, S.R., 2010. Building texture evolution networks for deformation processing of polycrystalline fcc metals using spectral approaches: applications to process design for targeted performance. *Int. J. Plasticity* 26, 1183–1194.
- Taylor, G.I., 1938. Plastic strain in metals. *J. Inst. Metals* 62, 307–324.
- Van Houtte, P., Delannay, L., Samajdar, I., 1999. Quantitative prediction of cold rolling textures in low-carbon steel by means of the LAMEL model. *Textures Microstruct.* 31, 109–149.
- Yoo, M.H., 1968. Slip modes of alpha uranium. *J. Nucl. Mater.* 26, 307–318.